Full Length Article

# Full-scale pullout tests of rock anchors in a limestone quarry focusing on bond failure at the anchor-grout and grout-rock interfaces

Bjarte Grindheim [a], Charlie C. Li [a,*], Are Håvard Høien [b]

[a] *Department of Geoscience and Petroleum, Norwegian University of Science and Technology (NTNU), Trondheim, Norway*
[b] *Norwegian Public Roads Administration (NPRA), Bergen, Norway*

## ARTICLE INFO

## ABSTRACT

Rock anchors are a common safety measure for stabilising large-scale infrastructure, such as bridge towers, retaining walls, rock slopes and windmills. There are four principal failure modes for rock anchors: (a) tensile failure of the steel anchor, (b) anchor-grout interface failure, (c) grout-rock interface failure, and (d) rock mass uplift. Field tests were performed in a limestone quarry. These tests were designed to test failure modes B and C through pullout. In the tests of failure mode B, the shear stress on the anchor-grout interface is the largest at the top of the grout column and attenuates towards the distal end for small loads. The shear stress becomes uniformly distributed when the applied load is approximately 50% of the ultimate pullout load. The anchors designed to test failure mode C were installed with an endplate and had a higher toughness than the straight bar anchors. The shear stress on the grout-rock interface is the largest at the endplate and attenuates upward before slip starts along the interface. When the ultimate pullout load is reached, and the grout column starts to slip, the shear stress is approximately constant. The bond shear strength on the anchor-grout interface was approximately 20% of the uniaxial compressive strength of the grout, and the bond strength of the grout-rock interface was around 5% for that of the grout. The grout-rock interface is likely determined by whichever is weaker, the grout or the rock.

© 2023 Institute of Rock and Soil Mechanics, Chinese Academy of Sciences. Production and hosting by Elsevier B.V. This is an open access article under the CC BY license (http://creativecommons.org/licenses/by/4.0/).

## 1. Introduction

Rock anchors are used to stabilise large-scale infrastructure, such as bridge towers, retaining walls, rock slopes and windmills. Rock anchors fulfil three basic functions. They provide a stabilising force on the structure in the direction of the anchor. The prestress applied to the anchor stresses the ground, which consolidates, strengthens, and improves the mechanical properties of the ground. The structure gets prestressed by the anchor, which unites it with the underlying ground (Hobst and Zajíc, 1983). Benmokrane and Ballivy (1991) stated that anchors also ensure longer stability of retained structures.

Tayeh et al. (2019) and Brown (2015) indicated that the application of rock anchors requires knowledge and understanding of the behaviour of the anchors for appropriate use, which demands information on their failure modes, strengths, load, displacement,

and steel relaxation characteristics. Rock anchors can fail in one of four modes: (a) tensile failure of the steel anchor, (b) pullout of the anchor from the grout (anchor-grout interface failure), (c) grout-rock interface failure, and (d) rock mass uplift (Littlejohn and Bruce, 1977). An anchoring system is only as strong as the weakest mode, and sufficient capacity must be ensured for all failure types (Pease and Kulhawy, 1984; Kim and Cho, 2012; Brown, 2015).

Field tests of rock anchors are performed to determine the uplift capacity and the minimum embedment depth required to prevent failure under in situ conditions with full-scale anchors (Ismael et al., 1979; Ismael, 1982). Full-scale field tests are also used to verify that designs have an adequate safety margin under the conditions in which the production anchors will be installed. These tests are recommended because they involve all the construction steps and increase the understanding of the anchor performance (Scott and Bruce, 1992). Full-scale field testing of anchors is performed for two reasons: (a) confirmation that the specific anchor performs as expected in the ground type and other environmental conditions, and (b) that the components of the selected anchor meet the design requirements and perform satisfactorily (Xanthakos, 1991). The most common tests performed are pre-

contract tests. These tests should prove beyond a reasonable doubt that the anchors can be constructed reasonably and will function as intended under the known conditions at the site (Hanna, 1982). Such testing can indicate errors in the design and installation of anchors and should, therefore, always be performed (Hobst and Zajíc, 1983).

The practical applicability of rock anchors has been demonstrated through full-scale tests (Kim and Lee, 2005). Multiple researchers have tested the failure modes of rock anchors in the field. General full-scale pullout tests have been conducted by Littlejohn et al. (1978) on carboniferous strata, Scott and Bruce (1992) on shaley sandstone, Weerasinghe and Littlejohn (1997) on mudstone, and Kim and Lee (2005) on a variety of rock types. Bruce (1976) conducted many field measurements during pullout trials, which were later analysed by Pease and Kulhawy (1984) and Panton et al. (2015). Kim and Cho (2012) designed pullout tests to test failure modes A and B in limestone. Pullout tests designed to test mode C have been performed by Haberfield and Baycan (1997) on siltstone, Park et al. (2013) on biotite gneiss, Liu et al. (2017) on limestone, and Bryson and Giraldo (2019) on shale. Dados (1984) tested failure mode D on fractured granite. Ismael et al. (1979), Ismael (1982) and Thomas-Lepine (2012) have tested failure modes C and D on shale and limestone. Other full-scale pullout tests have been conducted by Xiao and He (2018) on inflatable and reusable anchors, and by Briaud et al. (1998); Vukotic et al. (2013) on soil anchors.
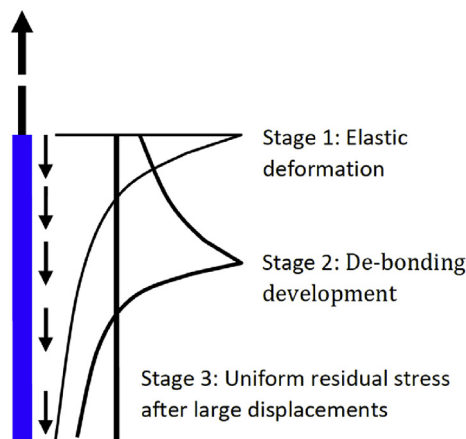
Three quantities are of direct interest in rock anchors: the applied load, the anchor head displacement, and the load distribution along the bonded length (Benmokrane et al., 1995). The design of rock anchors assumes a uniform distribution of loads along the bonded length of the anchor. Many former field and laboratory trials have shown this is not the case. The load is usually concentrated at the proximal end and attenuates towards the distal end (Liu et al., 2013), as shown in Fig. 1, which is based upon current theoretical models of load transfer from a grouted anchor. Some of the theoretical studies and field trials that have shown this are Hollingshead (1971), Pease and Kulhawy (1984), Li and Stillborg (1999), Park et al. (2013), Liu et al. (2017), and Bryson and Giraldo (2019). Most of those studies focused on the grout-rock bond, but the measurements are done along the anchor-grout interface. This assumes that the grout annulus is relatively thin, thus the shear stress measured at the anchor-grout interface is representative of the shear stress throughout the grout (Farmer, 1975).

**Table 1**
Rock mass rating of the limestone quarry by the Q-system from Pedersen (2014); location 5 is the test area.

| Location No. | RQD | $J_n$ | $J_r$ | $J_a$ | $J_w$ | SRF | Q-value | Quality |
|---|---|---|---|---|---|---|---|---|
| 1 | 84.6 | 6 | 3 | 1 | 1 | 2.5 | 16.92 | Good |
| 3 | 68.3 | 6 | 3 | 1 | 1 | 2.5 | 13.65 | Good |
| 4 | 64.7 | 6 | 3 | 1 | 1 | 1 | 32.35 | Good |
| 5 (test site) | 64.4 | 6 | 3 | 1 | 1 | 1 | 32.22 | Good |
| 6 | 58.4 | 6 | 3 | 6 | 1 | 1 | 4.87 | Fair |
| 7 | 58.9 | 6 | 3 | 2 | 1 | 1 | 14.72 | Good |
| Mean | 66.6 | 6 | 3 | 2 | 1 | 1.5 | 19.1 | Good |

Note: RQD = rock quality designation, $J_n$ = joint set number, $J_r$ = joint roughness number, $J_a$ = joint alteration number, $J_w$ = joint water reduction factor, and SRF = stress reduction factor.

**Table 2**
Joint set mapping at the test site.

| Joint set No. | Strike/dip | Average joint distance (cm) | Description |
|---|---|---|---|
| 1 | N60°E/ 70°NW | 30 | Bedding plane |
| 2 | N135°E/ 78°SW | 20 | Joints are planar and rough |
| 3 | N270°E/40°N | 40 | Joints are planar and rough |
| 4 | N36°E/80°SE | >100 | Joints are planar and rough |



**Fig. 1.** Three stages of stress transfer from anchor to rock: (1) Elastic deformation, (2) Debonding development, and (3) Uniform residual stress after large displacements.
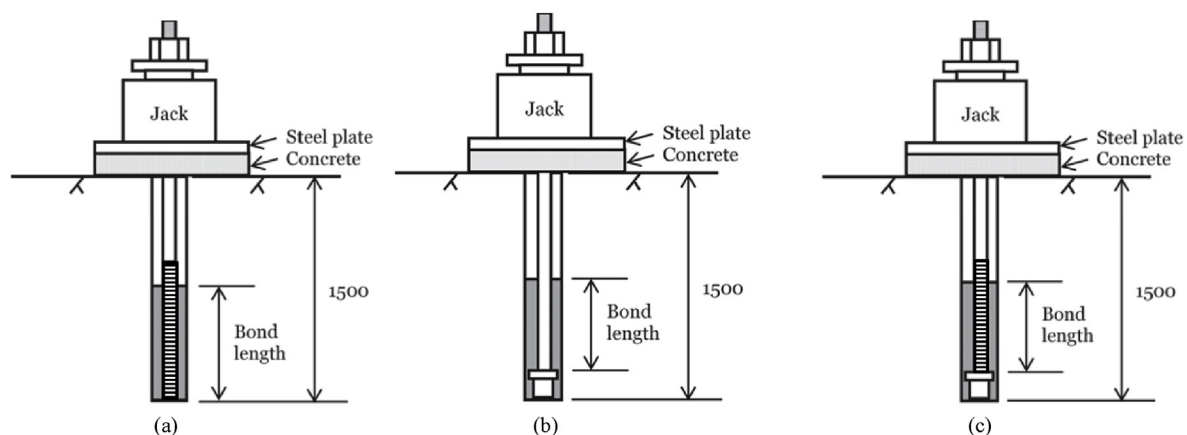


**Fig. 2.** Three configurations used for the tests: (a) Solid threaded bar, (b) Solid bar with endplate (the thread was debonded from the grout by a sleeve), and (c) Solid threaded bar with endplate.
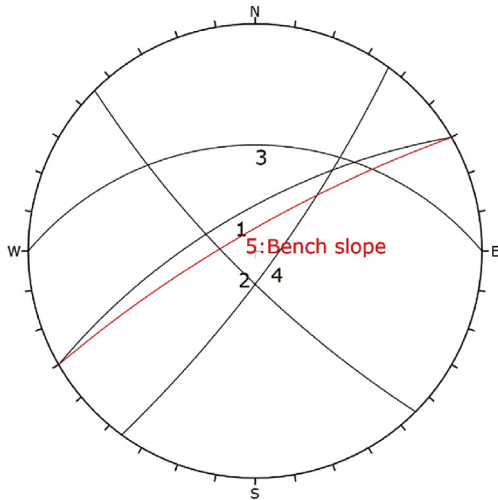
**Fig. 3.** Stereogram showing the strike and dip of the four joint sets in the rock mass at the test site and the bench slope.



**Fig. 6.** Hole layout in the field.

Monitoring the load distribution along the bonded length is uncommon, although it provides useful data on the load transfer, stress level, creep, or displacement of the bonded length. Electrical-resistance strain gauges are the most common way to monitor the stress distribution. Vibrating-wire gauges have also been used (Benmokrane et al., 1995). In recent years, a new method using fibre optic sensors has been tested to monitor the load distribution on soil anchors; the results appeared promising (Smet et al., 2019; Fabris et al., 2021). Field measurements can only be successful if the instruments are reliable and adequate (Benmokrane et al., 1995). Therefore, it is necessary to test fibre optic sensors on rock anchors in the field to verify the reliability of this monitoring method.

The current design methods against failure mode C have several deficiencies, which have been listed in a review by Brown (2015). The method assumes a uniform shear stress along the grout-rock interface, which Bruce (1997) said could lead to "extraordinarily and wastefully long bond zones". The design is often based on decades-old empirically based presumptive interface shear strength values. The progressive failure of the grout-rock bond is not recognised. The type of grout, borehole roughness and diameter, which all greatly affect the shear resistance, are not included in the design (Brown, 2015).
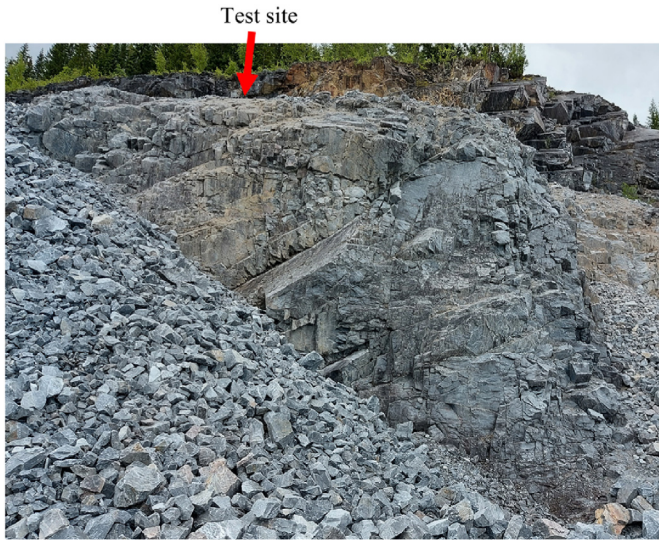


**Fig. 4.** Rock mass in the test site seen from the bench below, with clear signs of blast damage at the top of the bench closest to the test site.
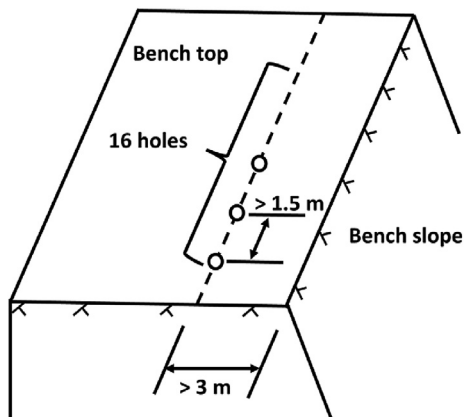


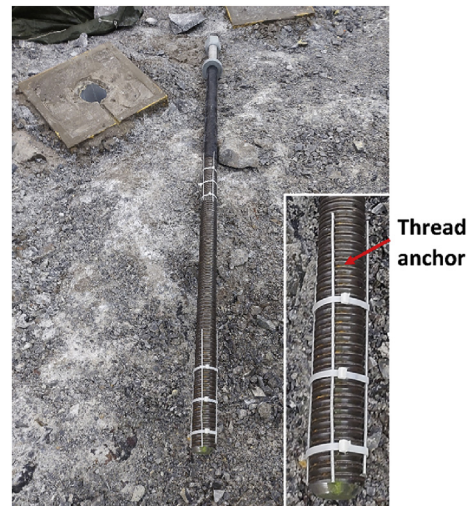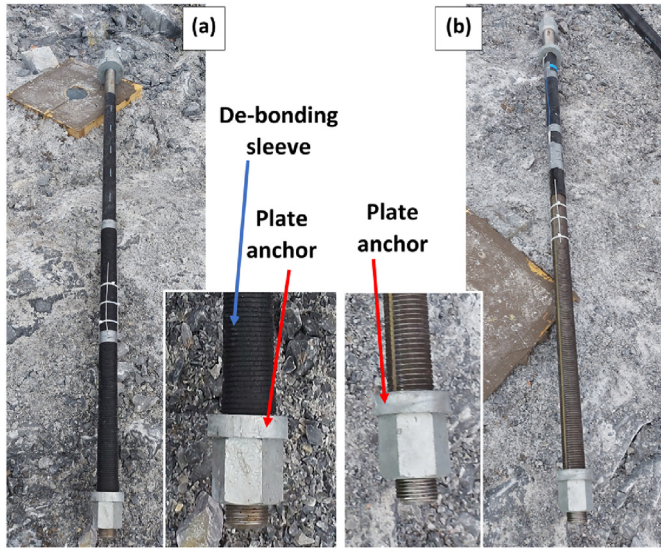**Fig. 5.** Sketch of hole layout.



**Fig. 7.** Example anchor used for test setup A (A-anchor).

**Fig. 8.** Examples of anchors used for tests B and C, (a) with plastic debonding sleeve (B-anchor) and (b) with a longitudinal grove instrumented with an FBG cable (C-anchor).

**Table 3**
Overview of anchor types and fibre instrumentation.

| Anchor No. | Bond length (mm) | W/C | Endplate | Debonding sleeve | FBG fibre instrumentation |
|---|---|---|---|---|---|
| 1A | 485 | 0.42 | | | On anchor |
| 2A | 523 | 0.42 | | | On anchor |
| 3A | 625 | 0.42 | | | |
| 4A | 730 | 0.42 | | | On anchor |
| 5A | 1080 | 0.42 | | | |
| 6A | 1100 | 0.42 | | | On anchor |
| 7A | 415 | 0.55 | | | |
| 1B | 315 | 0.42 | Yes | Yes | |
| 2B | 560 | 0.42 | Yes | Yes | In grout |
| 3B | 770 | 0.42 | Yes | Yes | In grout |
| 4B | 435 | 0.55 | Yes | Yes | |
| 1C | 280 | 0.42 | Yes | | |
| 2C | 625 | 0.42 | Yes | | On anchor |
| 3C | 840 | 0.42 | Yes | | On anchor |

Note: W/C represents the water-to-cement ratio.

This paper investigates the stress distribution along full-scale rock anchors on the anchor-grout and grout-rock interfaces during pullout and the load capacity of the interfaces when pulled to failure. The objective is to verify the validity of the current theoretical models for full-scale anchorage and to show the load transfer and failure mechanism along the grout-rock interface. Two types of anchors are used to force the bond failure to occur at either the anchor-grout or grout-rock interfaces. The tests were

conducted in the limestone quarry of Verdalskalk in Norway, which is a medium-hard rock mass. The anchors used have the same dimensions as those commonly used for foundation reinforcement in Norway. The stresses along the anchor and in the grout are monitored with fibre optic cables with fibre Bragg grating (FBG), a novel application for this technology. The test results and increased measurement quality are expected to improve our knowledge of some of the deficiencies that Brown (2015) listed and thereby enable improved rock anchor designs.

## 2. Test preparation

### 2.1. Testing plan

The field tests aimed to investigate the failure along the anchor-grout and grout-rock bond interfaces. A testing plan with three test setups was developed to investigate the bond failures through pullout, as shown in Fig. 2. All the tests, 14 in total, were carried out with 64-mm diameter bar anchors in 140-mm boreholes drilled to a depth of 1.5 m. The rock anchor in test setup A, as shown in Fig. 2a, is a type of threaded bar anchor that is currently used for rock anchoring in various rock engineering projects. The anchor could fail along either the anchor-grout or grout-rock interface. A critical embedment depth exists for this type of rock anchor. The anchor would be pulled out of the borehole when the bond length is shorter than the critical embedment length. An endplate was attached to the distal end of the bar in test setups B and C, as shown in Fig. 2b and c, aiming to force the failure to occur along the grout-rock interface to investigate the bond strength of that interface. For test B, the anchor stem was debonded by a polymer sleeve so that the applied load was entirely transferred to the endplate, while for test C, the applied load was partially carried by the bonded thread section so that the effect of the thread on the load transfer to the endplate was investigated. The bond length for tests B and C was defined as the grouted length above the endplate.

Optical fibres with FBG were used to measure the axial strains along the anchor and in the grout in the tests. An FBG is a quasi-distributed fibre-optic sensing technique. The optical fibres are designed to guide light within the fibres. Strain changes between measuring points will change the wavelength or intensity of the scattered, reflected, or transmitted light. Optoelectronic instruments can measure these changes.

Seven anchors were instrumented with FBG optical fibres in grooves to measure the axial strains along the anchor. Each fibre had 20 measuring points (FBGs) evenly distributed along the bond length of the anchor. The technique utilises a special phenomenon of the reflected light due to the Bragg grating on the optical fibre. The working principle of an optical fibre with FBGs is that each FBG reflects a narrow spectral part of the light centred at a certain wavelength, which is called the Bragg wavelength. The Bragg wavelength is strain and temperature dependent. Changes in strain

**Table 4**
The ultimate loads and average bond strengths of the A-anchors.

| Anchor No. | W/C | Bond length (mm) | Ultimate load | | Average bond strength (MPa) | | Load oscillation | Failure status |
|---|---|---|---|---|---|---|---|---|
| | | | Measured load (kN) | Load per meter (kN/m) | At anchor-grout | At grout-rock | | |
| 1A[a] | 0.42 | 485 | 1404 | 2895 | 14.4 | | Strong | Anchor-grout |
| 2A[a] | 0.42 | 523 | 1240 | 2371 | 11.79 | | Strong | Anchor-grout |
| 3A | 0.42 | 625 | 995 | 1592 | (7.92)[b] | 3.62 | Little | Anchor-grout-rock |
| 4A[a] | 0.42 | 730 | 1634 | 2238 | 11.13 | | Strong | Anchor-grout |
| 5A | 0.42 | 1080 | 1418 | 1313 | (6.53)[b] | 2.99 | Little | Anchor-grout-rock |
| 6A[a] | 0.42 | 1100 | 1484 | 1349 | | 3.07 | No | Grout-rock |
| 7A | 0.55 | 415 | 377 | 908 | | 2.07 | No | Grout-rock |

[a] The FBG strain sensors are on the anchors.
[b] It does not represent the bond strength of the anchor-grout interface and it is excluded from the calculation of the average bond strength of the interface.

**Table 5**
The ultimate loads and average bond strengths of the B-anchors.

| Anchor No. | W/C | Bond length (mm) | Ultimate load | | Mean grout-rock bond strength (MPa) | Bond status |
|---|---|---|---|---|---|---|
| | | | Measured load (kN) | Load per meter (kN/m) | | |
| 1B | 0.42 | 315 | 1084 | 3443 | (7.83)[b] | With debonding sleeve |
| 2B[a] | 0.42 | 560 | 1156 | 2064 | 4.69 | |
| 3B[a] | 0.42 | 770 | 1257 | 1633 | 3.71 | |
| 4B | 0.55 | 435 | 720 | 1654 | 3.76 | |

[a] The FBG strain sensors are placed in the grout.
[b] Excluded from the analysis because of the unusual post-peak behaviour due to overly short bond lengths.

**Table 6**
The ultimate loads and average bond strengths of the C-anchors.

| Anchor No. | W/C | Bond length (mm) | Ultimate load | | Mean grout-rock bond strength (MPa) | Bond status |
|---|---|---|---|---|---|---|
| | | | Measured load (kN) | Load per meter (kN/m) | | |
| 1C | 0.42 | 280 | 826 | 2951 | (6.71)[b] | No debonding |
| 2C[a] | 0.42 | 625 | 1031 | 1650 | 3.75 | |
| 3C[a] | 0.42 | 840 | 1376 | 1638 | 3.72 | |

[a] The FBG strain sensors are on the anchors.
[b] Excluded from the analysis because of the unusual post-peak behaviour due to overly short bond lengths.
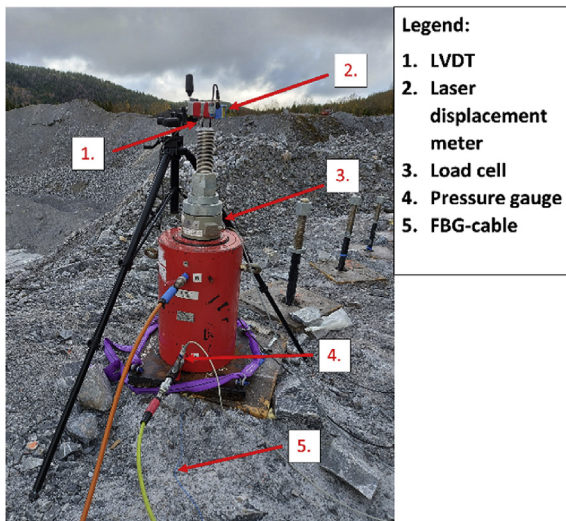


**Fig. 9.** Test setup with instrumentation for an anchor.

will alter the Bragg wavelength, and these changes in the Bragg wavelength can be measured to calculate the strains (Zhu et al., 2017). In three tests, optical fibres were embedded within the grout close to the borehole wall during anchor installation in order to monitor the loading process of the grout and the debonding at the grout-rock interface. All the measurements were continuously logged at 10 Hz with a FiSpec FBG X100 interrogator from FiSens, Braunschweig, Germany.

### 2.2. Test site

The pullout tests were performed in the open pit limestone quarry of Verdalskalk AS in Tromsdalen, Norway. This quarry is one of the largest and purest limestone occurrences in Europe. This limestone occurrence is estimated to contain 3 billion tonnes of limestone useable for all purposes (Storli, 2021). The test site was in a corner of the quarry with strong unweathered limestone. The rock is homogeneous, with an average uniaxial compressive strength (UCS) of 75 MPa, ranging from 36.6 MPa to 87.8 MPa. The limestone quarry and test area were mapped with the Q-system by Pedersen (2014), and the rock mass in the test area was rated 32 and was of good quality. The rock mass quality of the quarry is summarised in Table 1; location 5 is the test area. The rock joints in the test area were mapped and measured. Four joint sets were found in the rock mass; the strike and dip of these joint sets together with the bench slope nearby are shown in Table 2 and the stereogram in Fig. 3. All the joints at the test site were planar and rough. Since the mine was active, it was evident that the rock mass was blast damaged. Fig. 4 shows the rock mass in the test site from a bench below the test site; the blast damage is close to the top of the bench.

The holes for the rock anchors were pneumatically drilled with a 140-mm diameter button bit to a depth of 1.6 m. They were placed with a minimum spacing of 1.5 m and a minimum distance of 3 m to the bench crest, as illustrated in Fig. 5 and shown in Fig. 6.

### 2.3. Rock anchors

Two types of anchors were used in the tests. Both anchor types were 64 mm in diameter. The first type, the A-anchor, was made of normal solid bar with a length of 2.5 m and 1.2 m of M68 thread at the bottom, as shown in Fig. 7, and was used in test setup A. The second type, used for test setups B and C, was the same as the first, except the diameter of a short section of the distal thread was reduced to 56 mm to attach a washer 100 mm in diameter, which worked as an endplate anchor, as shown in Fig. 8. The head thread of the anchors was attached with a washer and a nut. The anchor steel had Young's modulus of 200 GPa with a nominal tensile strength of 1000 MPa (i.e. an ultimate load of 3217 kN for the 64-mm stem).

The B-anchors, used in test B, were wrapped with debonding pipe to ensure that the load was transferred to the endplate. The debonding pipes were plastic pipes with an adjustable diameter (50−100 mm), which were tightened around the anchors to cover the M68 thread above the endplate, as shown in Fig. 8a). An overview of all the anchors is given in Table 3.

### 2.4. Anchor installation

The rock surface around the bored holes was uneven and rough. Formwork with dimensions 50 cm × 50 cm was placed around the anchors to level the surface. A 150-mm diameter concrete cardboard casting pipe was placed around the borehole. Construction foam was used to fasten and seal the formwork and cardboard pipe to the rock surface. The lower half of the formwork was filled with rocks, and cementitious grout was poured over it until it was fully filled. Then, the top surface was evened out, and the concrete was left to harden for 7 d prior to anchor installation.

After the concrete platforms had hardened, the installation of the anchors commenced. The over-drilled bottom of the boreholes was filled with gravel until the length from the platform surface to the bottom of the borehole was 1.6 m. Short steel wires were partially fastened with zip ties around the anchor stem in two positions toward the bottom of the stem. The unfastened parts of the wires were bent outward. The anchors were lifted using an excavator and placed in the boreholes. The outward extending wires centred the anchor stems in the boreholes. Then, the grout hose was inserted into the bottom of the hole, and the required volume of cementitious grout was pumped into the hole. For each batch of grout, two cubes and two cylindrical samples were casted
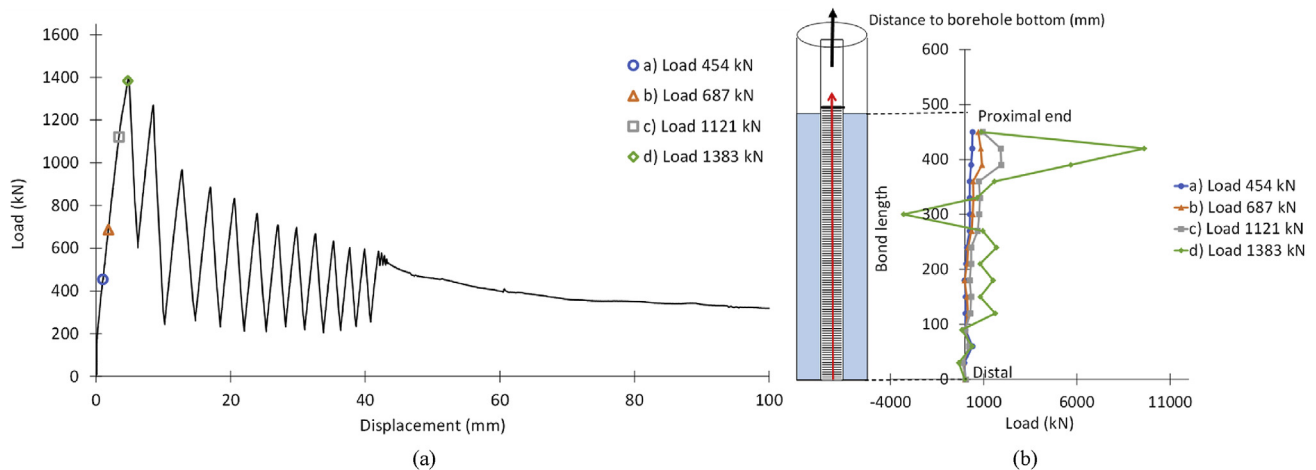
**Fig. 10.** Pullout test results for anchor 1A: bond length 485 mm and $W/C = 0.42$: (a) Load vs. displacement plot, and (b) Load distribution along the anchor. Ultimate pullout load $P_{ult} = 1404$ kN.

for quality control. The bond length of the anchors was checked by measuring the depth of the un-grouted portion of the holes after the grout hardened. Two water-to-cement ($W/C$) ratios, 0.42 and 0.55, were used for the grout in order to examine the influence of the grout strength on the bond strength. The average UCS of the grout after hardening for 28 d was 60.5 MPa for $W/C = 0.42$ and 37.8 MPa for $W/C = 0.55$, respectively. The average strength after hardening for 7 d for $W/C = 0.42$ was 45.4 MPa. The bond lengths and $W/C$ ratios are summarised in Table 4 for A-anchors, in Table 5 for B-anchors, and in Table 6 for C-anchors.

The FBG fibres were embedded in the grout by fastening them to the back side of plastic cable concealers with adhesive and placing the cable concealers in the borehole after the anchor had been placed close to the borehole wall. The top side of each cable concealer was perforated with a knife, which allowed the cementitious grout to fully cover the cable concealer when the borehole was filled with grout. The plastic material had a low stiffness and was assumed to follow the deformation of the grout surrounding it.

### 2.5. Test arrangement and procedure

The test setup together with instrumentation is shown in Fig. 9. A 5-cm thick 500 mm × 500 mm steel plate was placed to evenly distribute the load over the concrete platform. A 3500-kN hydraulic jack sat on the top of the steel plate. The hydraulic jack had a stroke of 300 mm and a push area of 499 cm². It weighed 397 kg and was moved between anchors with an excavator. A gasoline-driven hydraulic pump drove the jack with a maximum pressure of 200 bar. The pressurised oil was sent to the jack through a booster unit which could increase the pressure to 700 bar. A pressure gauge was used to measure the oil pressure, which was used to calculate the load applied to the anchor.

A 1500-kN load cell was placed at the head of the rock anchor to measure the pull load applied to the anchor. A tripod was placed on the solid ground beside the concrete plate. A thread extensometer (LVDT) and a laser meter were fixed to the tripod. The LVDT was attached to the anchor head to measure the pull displacement of the anchor. The settling of the hydraulic jack was monitored by the laser meter to ensure the platforms were correctly casted.

The anchors were loaded in two ways. The first two anchors, 1B and 1C, were loaded stepwise in a force-controlled mode with steps of 100-kN at the beginning and 50-kN steps when the load-deformation curve started to bend (i.e. the transition from elastic

to plastic deformation). This process was followed to stably control the loading process and to better understand the elastic and plastic deformation of the anchors. Initially, each load step was held for 3–5 min to allow the displacements to settle. Unfortunately, the jack could not hold constant pressure, and the pressure dropped when the pump stopped. Loading-unloading cycles were also conducted to study the hysteresis behaviour of the anchors in detail. The rest of the anchors were loaded slowly and monotonically with load rates of 5–10 kN/s until the ultimate load capacity was passed and the steady residual capacity of the anchors was reached. All the pullout tests were performed between 18 and 21 October 2021.

## 3. Results and analysis

### 3.1. A-anchors

Seven anchors in this category were pull tested. The load-displacement curves and the load distribution along the bond length of the anchors are presented in Figs. 10–16 for the A-anchors from short to long bond lengths. The loads along the anchor, such as those presented in Fig. 11b, were calculated from the strains measured by the FBGs. Positive loads are extensive (e.g. in Fig. 11b), and negative loads are compressive (e.g. in Fig. 19b). The ultimate loads are presented in Table 4 from short to long bond length.

#### 3.1.1. Load capacity and average bond strength

The pattern of the load-displacement curve is similar for all A-anchors. The pull load reached its maximum after a very small displacement, around 5 mm. The load oscillated in five of the seven anchors in the post-peak stage, as shown in Fig. 10. The load oscillation was periodic, with a displacement of around 4 mm for every load drop, which is equal to the pitch (the tooth spacing) of the anchor thread (see Fig. 7). This behaviour was particularly clear for anchors 1A (Figs. 10a) and 4A (Fig. 13a). In this case, the load oscillation appears to be caused by the slip of the anchor thread in the grout; in other words, the failure was at the anchor-grout interface. The oscillation disappeared, and smooth slip continued when the anchor-grout interface was flattened.

The oscillations of anchors 3A (Figs. 12) and 5A (Fig. 14) were very weak and lasted for only a short displacement. The load oscillation implies that slip first occurred at the rough anchor-grout interface. These anchors had 1–2 mm larger displacement at peak load than the other A-anchors with oscillation, which also implies
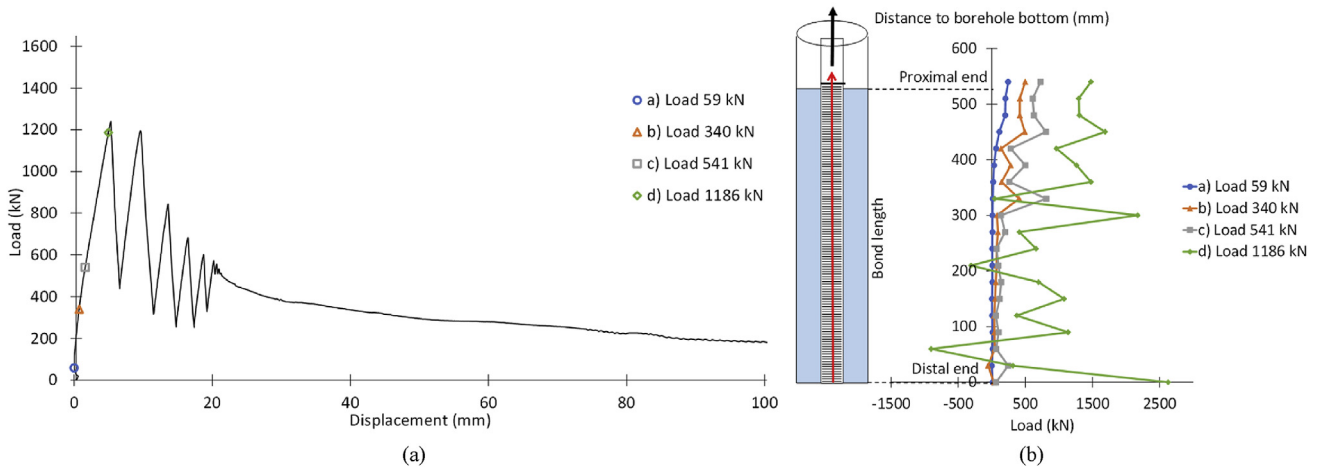
**Fig. 11.** Pullout test results for anchor 2A: bond length 523 mm and $W/C = 0.42$: (a) Load vs. displacement plot, and (b) Load distribution along the anchor. Ultimate pullout load $P_{ult} = 1240$ kN.
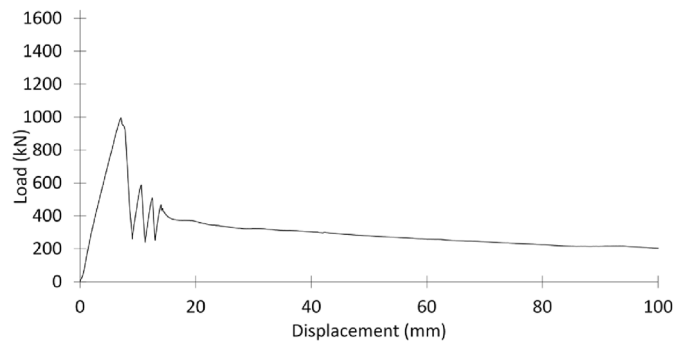


**Fig. 12.** Pullout load vs. displacement plot for anchor 3A: bond length 625 mm and $W/C = 0.42$. Ultimate pullout load $P_{ult} = 995$ kN.

slip on the grout-rock interface before oscillation started. The ultimate loads of the two anchors were lower than those of the two strongly oscillating anchors, 1A and 4A, in kN/m of the bond length. That means that the shear failure might not solely occur at the anchor-grout interface, but failure might also occur at the grout-

rock interface. In other words, both the anchor-grout and grout-rock interfaces might fail in anchors 3A and 5A.

No oscillations at all were observed for anchors 6A (Figs. 15a) and 7A (Fig. 16). No oscillation implies no slip at the thread, anchor-grout interface, so that the shear failure might occur at the grout-rock interface.

The intensity of the load oscillation of anchor 2A (Fig. 11a) is in between the anchors subjected to strong oscillations (1A and 4A) and the anchors to weak oscillations (3A and 5A). Both the anchor-grout and grout-rock interfaces might fail, but the failure might dominate at the anchor-grout interface because of its high ultimate load per metre of bond length.

Based on the above analysis, it is inferred that the failure was at the anchor-grout interface for anchors 1A, 2A and 4A, at the grout-rock interface for anchors 6A and 7A, and at both for anchor 3A. The bond (shear) strengths of the anchors were then calculated at the anchor-grout interface using the anchor diameter of 64 mm and at the grout-rock interface using the hole diameter of 140 mm, as presented in Table 4. The average grout-rock bond strengths in Table 4 are not based upon pure shear between the grout and rock, and they also include some crushing of the grout. The bond strengths of anchors 3A and 5A are presented at both the anchor-
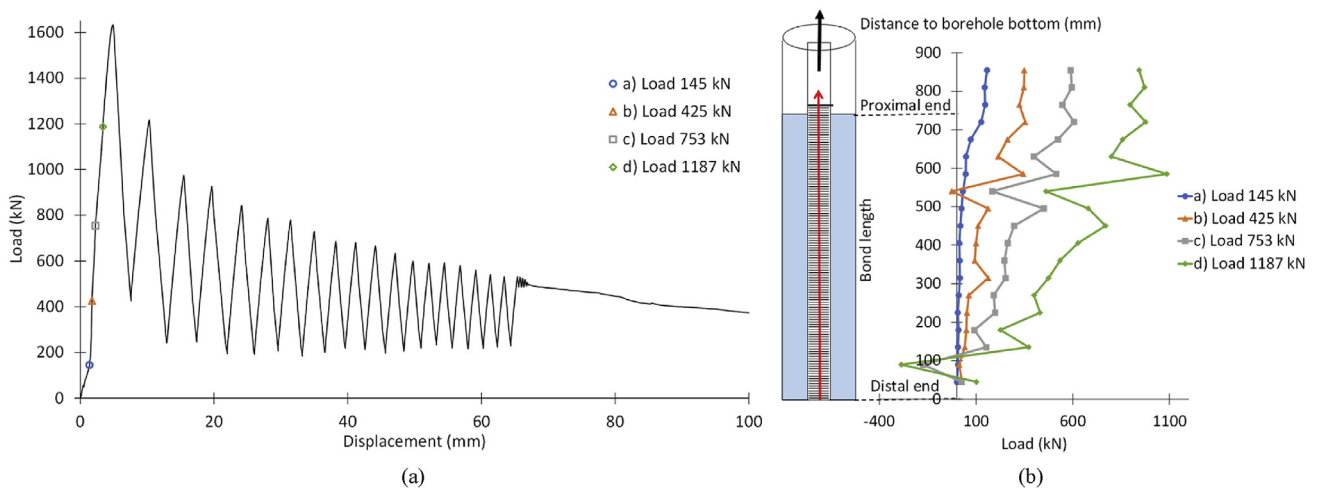


**Fig. 13.** Pullout test results for anchor 4A: bond length 730 mm and $W/C = 0.42$: (a) Load vs. displacement plot, and (b) Load distribution along the anchor. Ultimate pullout load $P_{ult} = 1634$ kN.

grout interface and the grout-rock interface because failure might occur at both interfaces. However, the failure may not fully develop at the anchor-grout interface when the grout-rock bond fails along the grout-rock interface. The weak load oscillations of the two anchors are evidence of the incomplete failure at the anchor-grout interface. Therefore, the calculated values for the bond strength of the two anchors at the anchor-grout interface, 6.53 MPa and 7.92 MPa, are questionable.

Except for anchors 3A and 5A, as discussed above, the bond strengths of the three anchors that failed at the anchor-grout interface (anchors 1A, 2A and 4A) vary within a narrow range of 11.13−14.4 MPa (mean 12.44 MPa). The UCS of the grout with $W/C = 0.42$ is 60.5 MPa. Therefore, the mean bond strength of the anchor-grout interface is 20.56% of the UCS of the grout. The bond strengths of the three anchors that failed at the grout-rock interface (anchors 3A, 5A and 6A) are also quite consistent, varying over a range of 2.99−3.62 MPa (mean 3.23 MPa).

Anchor 7A was installed with grout having a $W/C$ ratio of 0.55. The grout-rock bond strength of the anchor is 2.07 MPa, i.e. lower than the bond strength, with a $W/C$ ratio of 0.42. This is reasonable because the strength of the grout with $W/C = 0.55$ ($UCS = 37.8$ MPa) is lower than that of the grout with $W/C = 0.42$ ($UCS = 60.5$ MPa). The grout, the rock, or both may fail at the grout-rock interface. A piece of hardened grout was removed from the hole after the test of anchor 7A. The surface of the grout column was damaged (Fig. 17b). The UCS of the limestone varies in a range of 36.6−87.8 MPa with a mean value of 75 MPa. The rock is stronger than the grout with $W/$ $C = 0.55$ ($UCS = 37.8$ MPa), thus the damage was in the grout. For the grout with $W/C = 0.42$, the damage may have been in the grout because it ($UCS = 60.5$ MPa) was weaker than the rock. The tests showed that the bond shear strength of the grout-limestone interface is 5.34% of the UCS of the grout with $W/C = 0.42$ and 5.48% of the UCS of the grout with $W/C = 0.55$. These two ratios only differ by a very small margin.

### 3.1.2. Load distribution along the bond length of the anchor

The axial load along the anchor in the bonded section was measured by the FBGs in four of the A-anchors. The load distribution in anchor 1A is presented in Fig. 10b at four applied load levels in the pre-peak stage. The grout top is 485 mm from the distal end of the anchor. At approximately one-third of the ultimate applied load, i.e. 454 kN, the load in the anchor was maximal at the top of the grout and decreased towards the distal end. The load increased with an increased applied load in a 100-mm section at the proximal end of the bond length until it reached 1383 kN, i.e. close to the ultimate load. The top 100 mm of the grouted anchor section received most of the applied load, but the load-bearing mobilised section was approximately 200 mm from the top of the grout to 250 mm from the distal end.

Fig. 11b shows the load distribution of anchor 2A at four levels of applied load. The distribution was similar to that in anchor 1, except at 1186 kN, close to the ultimate load. The load-mobilised section was the top 220 mm from the proximal end to approximately 300 mm from the distal end. It is hard to interpret the load distribution at the load level of 1186 kN because of the fluctuation of the measured load. The FBGs are either damaged or disturbed at that load level. It appears that the entire 523-mm long bond length of the anchor was mobilised at that level.

The load distributions of anchors 4A and 6A were similar and are presented in Fig. 13b and 15b, respectively, at four levels of applied load. In these two anchors, the maximum load occurred at the top of the bond length and attenuated rapidly towards the distal end at low levels of applied load. The entire bond length was mobilised to carry the load at load levels close to the ultimate applied load.

### 3.2. B-anchors and C-anchors

The load−displacement curves and the load distribution along the bond length of the anchors or within the grout are presented in Figs. 18−21 for the B-anchors, and Figs. 22−24 for the C-anchors,
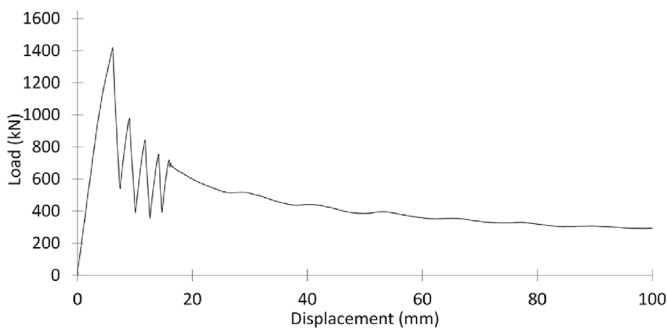


**Fig. 14.** Pullout load vs. displacement plot for anchor 5A: bond length 1080 mm and $W/C = 0.42$. Ultimate pullout load $P_{ult} = 1418$ kN.
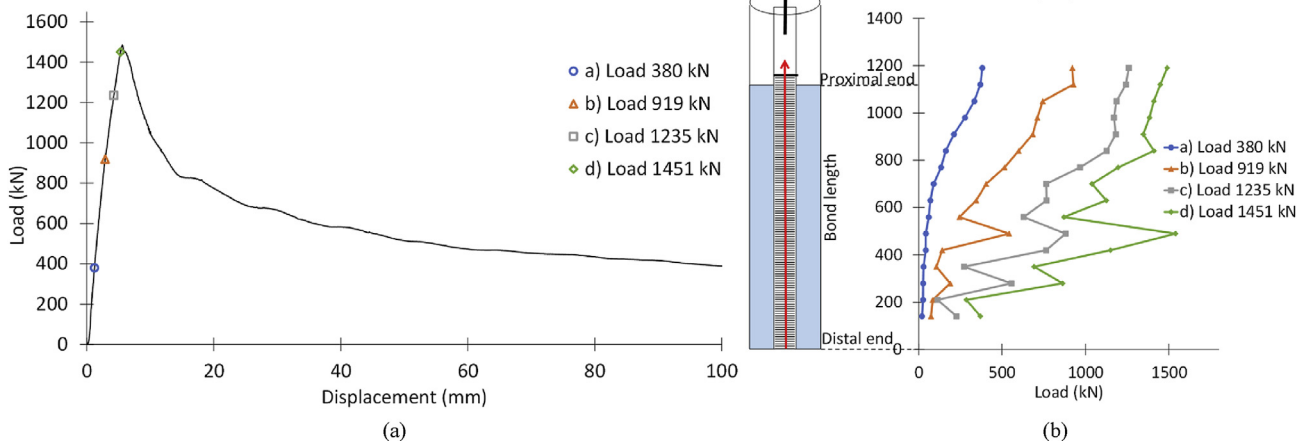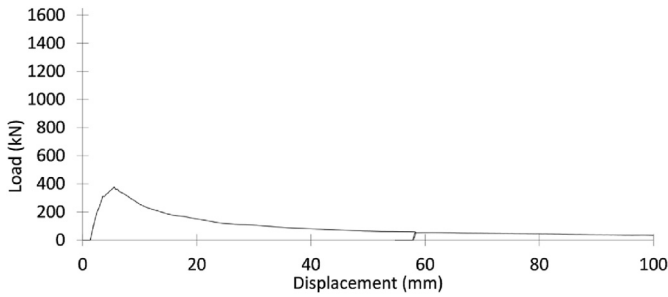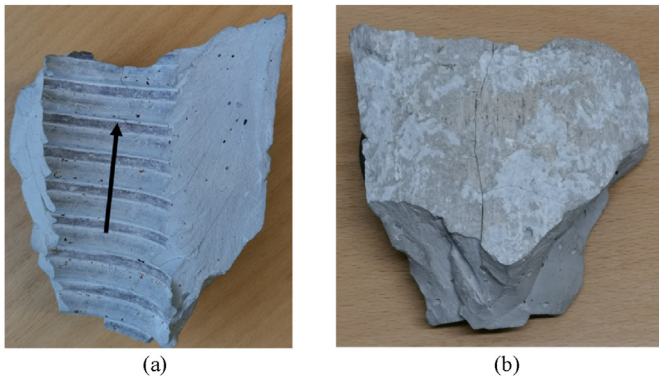


**Fig. 15.** Pullout test results for anchor 6A: bond length 1100 mm and $W/C = 0.42$: (a) Load vs. displacement plot, and (b) Load distribution along the anchor. Ultimate pullout load $P_{ult} = 1484$ kN.
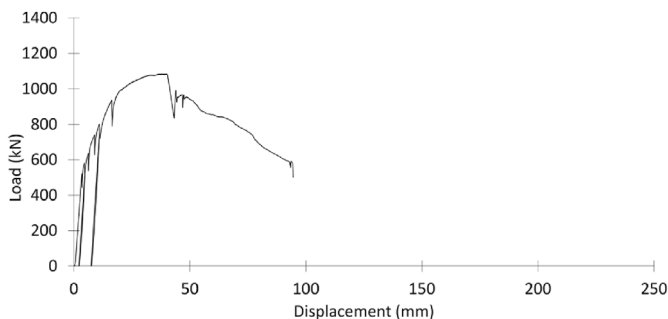
**Fig. 16.** Pullout load vs. displacement plot for anchor 7A: bond length 415 mm and $W/C = 0.55$. Ultimate pullout load $P_{ult} = 377$ kN.



**Fig. 17.** A hardened grout fragment from anchor 7A that was pulled out of the borehole: (a) The side facing the anchor, and (b) The side facing the borehole wall. The arrow indicates the direction the anchor moved during the pull test.

from short to long bond lengths. The load drops in some of the B- and C-anchors at displacements around 220 mm, such as in Fig. 19a, were due to unloading at the end of the stroke of the jack. The anchor was reloaded after stroke adjustments. The load displacement in the second loading cycle is only partially shown in the figure.

The B-anchors were divided into two groups for analysis. The first group included three anchors, 1B, 2B and 3B. The second group had only one anchor, 4B, which was debonded in the thread section but had a higher $W/C$ ratio (0.55) than the other B-anchors (0.42). The group of C-anchors (Fig. 8b) included three anchors, 1C, 2C and 3C. The main objective of the B- and C-anchor tests was to test the bond strength of the grout-rock interface. Debonding was not used for the C-anchors to examine how the thread bond affects the load transfer to the plate at the distal end of the anchor.



**Fig. 18.** Pullout load vs. displacement plot for anchor 1B: bond length 315 mm with debonding sleeve and $W/C = 0.42$. Ultimate pullout load $P_{ult} = 1084$ kN.

The clearance between the borehole (diameter 140 mm) and the endplate (diameter 120 mm) of the B-anchors is only 10 mm on each side. The yielding displacement measured on the anchor should equal the displacement of the grout column when the small amount (mm) of elastic elongation of the anchor stem is neglected.

### 3.2.1. Load capacity and average bond strength

The load–displacement curves of all anchors with endplate grouted with $W/C = 0.42$ are similarly nonlinear in the pre-peak stage, as shown in Figs. 18–20 and 22–24. However, the post-peak behaviour of anchors 1B and 1C differed from that of the other anchors because their loads dropped much more quickly in the post-peak stage, as shown in Figs. 18 and 22. The bond lengths of the two anchors, 315 mm for 1B and 280 mm for 1C, were the shortest among the B- and C-anchors. The short bond lengths resulted in the fragile post-peak behaviour of the two anchors. Therefore, the test results of the two anchors are not reliable, and they were excluded in the subsequent analysis of the B- and C-anchors.

The bond lengths of the other four B- and C-anchors, 2B, 3B, 2C and 3C, varied from 560 mm to 840 mm. These anchors behaved similarly in the post-peak stage, as shown in Fig. 19a, 20a and 23a and 24a. The load remained slightly smaller than the ultimate load for a long displacement after passing the ultimate load. In other words, these anchors were tough. All the B- and C-anchors failed at the grout-rock interface along the borehole wall. It was observed in the field that the grout columns were pulled upward and slid along the borehole during the tests. When anchors 1B and 1C were excluded, the mean grout-rock bond shear strengths of the remaining four B- and C-anchors for the grout with $W/C = 0.42$ were similar, varying from 3.71 MPa to 4.69 MPa with a mean value of 3.97 MPa, as shown in Tables 5 and 6 The mean grout-rock bond strengths in Tables 5 and 6 are not based upon pure shear between the grout and rock, and they also include some crushing of the grout. The mean bond strength was 6.56% of the UCS of the grout (60.5 MPa).

Anchor 4B was installed using grout with a higher $W/C$ (0.55). Its load–displacement behaviour was comparable to the other B- and C-anchors, as shown in Fig. 21. The bond shear strength of this anchor was 3.76 MPa (see Table 5) at the grout-rock interface, which is similar to that of the B-anchors installed in the grout with $W/C = 0.42$. The noticeably high bond strength of anchor 4B may be due to the scale effect. The bond length of anchor 4B was only 435 mm, shorter than all four valid B- and C-anchors installed in the grout with $W/C = 0.42$.

### 3.2.2. Strains in the grout column

The strains in the grout columns of anchors 2B and 3B were measured by FBGs. The load was transferred directly to the endplate because the anchoring thread was debonded by the sleeve. The pull load in the anchor stem was converted to compressive load in the grout column via the plate at the distal end of the anchor, and the grout column was pushed upward. The load was then transferred to the rock mass at the grout-rock interface. The variation of the compressive load in the grout column represents the distribution of the shear stress to the grout-rock interface along the borehole length and manifests where the anchor load is transferred to the rock mass. Theoretically, the measured strains can be converted to stress or load by Hooke's law, but bias could be generated when the grout fractured and was no longer a linear elastic medium and there are some uncertainties in the measurements related to FBG fibres. The grout in the borehole was fractured, at least in the proximity of the endplate. Because of that consideration, the measured strains are directly presented in Fig. 19b and 20b for
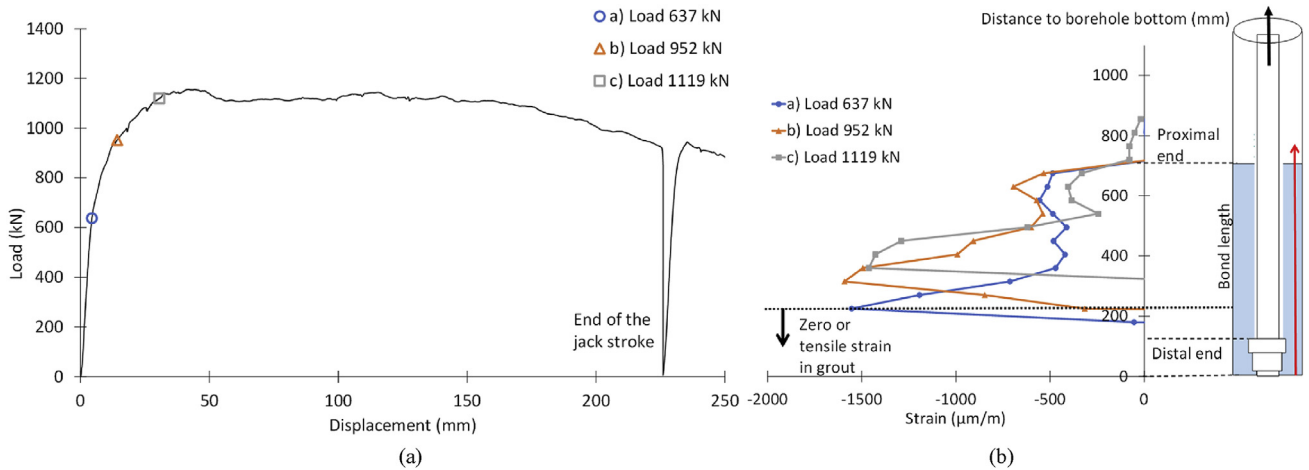
**Fig. 19.** Pullout test results for anchor 2B: bond length 560 mm with debonding sleeve and $W/C = 0.42$: (a) Load vs. displacement plot, and (b) Strain distribution in the grout column. The load drop at around 230 mm marks the end of the stroke of the jack. Ultimate pullout load $P_{ult} = 1156$ kN.

anchors 2B and 3B. Qualitatively, a high strain is equivalent to a high stress or load.

The strains in the grout column of anchor 2B are presented for three load levels during the pre-peak stage in Fig. 19b. The load (637 kN) was slightly more than 50% of the ultimate load (1155 kN) and was associated with the beginning of the nonlinear displacement. The other two load levels, 952 kN and 1119 kN, are approximately 80% of, and close to, the ultimate load. At the load of 637 kN, the compressive strain in the grout was maximal at 210 mm from the distal end. The compressive strain dropped linearly to around $500 \times 10^{-6}$ at a distance of 350 mm. The strain remained at $500 \times 10^{-6}$ until it abruptly dropped to zero at the top of the grout column. The strain distribution pattern along the grout column remained similar at the other two load levels, but the position of the maximum compressive strain moved upward with increased applied load. The strain was zero or tensile in the grout below the position of the maximum compressive strain.

The strains of anchor 3B (Fig. 20b) fluctuated greatly, possibly because of disturbances to the FBGs. However, all curves at the three load levels show that the compressive strain in the grout tended to attenuate toward the top of the grout column.

The grout strain curves of these two anchors show that the grout column had the greatest load at the bottom; most of the anchor load was transferred to the rock mass at the bottom of the borehole.

### 3.2.3. Load distribution along the bond length of the anchor

As mentioned previously, anchors 2C and 3C were not debonded in the anchoring thread section at their distal ends. The FBGs were instrumented on the anchor stem in anchors 2C and 3C so that the FBG measurements were the strain and load distributions along the thread anchor. The load distributions of anchor 2C are presented in Fig. 23b at four applied load levels (471, 757, 920 and 995 kN). The first three loads were in the loading stage before the first peak load (946 kN) was reached, while the fourth was in the stable yielding stage. At a load of 471 kN, the load in the anchor was maximal at the top of the grout column, 625 mm from the endplate, and attenuated toward the distal end. The load appeared to have dropped to almost zero at the endplate; the endplate did not carry any load. At the applied load of 757 kN, the maximum load remained at the top of the grout, but the load rapidly dropped to around 500 kN and remained at that level from 320 mm above the endplate and below. This result implies that the load transferred to the endplate was approximately 460 kN and the load carried by the thread was $757 - 460 = 297$ kN. At an applied load of 920 kN, the load distribution pattern was similar to that at 757 kN, but the load transferred to the endplate was around 740 kN. The load on the thread decreased, i.e. $920 - 740 = 180$ kN. At these three applied load levels, the anchors only moved from 3 mm to 6 mm, implying that the grout column had just begun to move upward. At the fourth level (995 kN), the anchor and
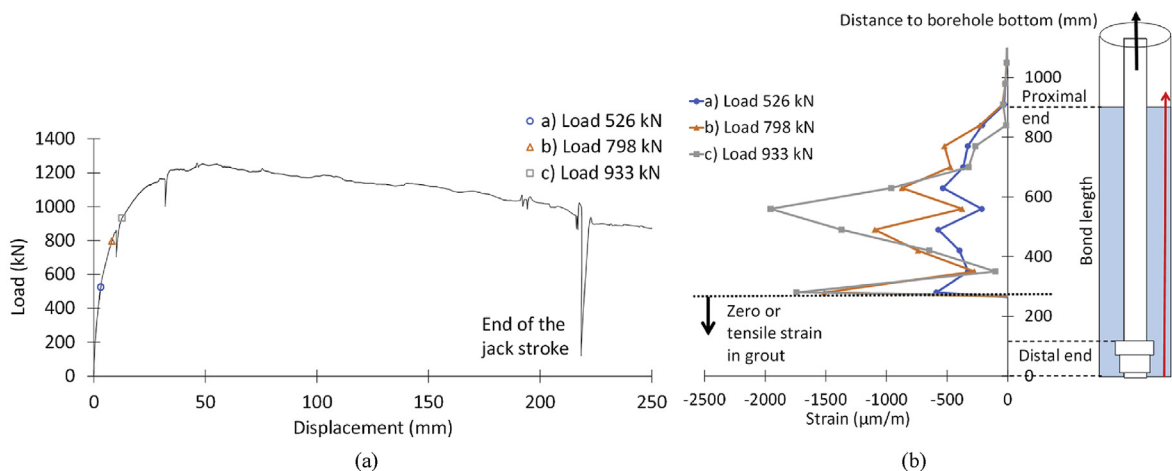


**Fig. 20.** Pullout test results for anchor 3B: bond length 770 mm with debonding sleeve and $W/C = 0.42$: (a) Load vs. displacement plot, and (b) Strain distribution in the grout column. The load drop at around 220 mm marks the end of the stroke of the jack. Ultimate pullout load $P_{ult} = 1257$ kN.
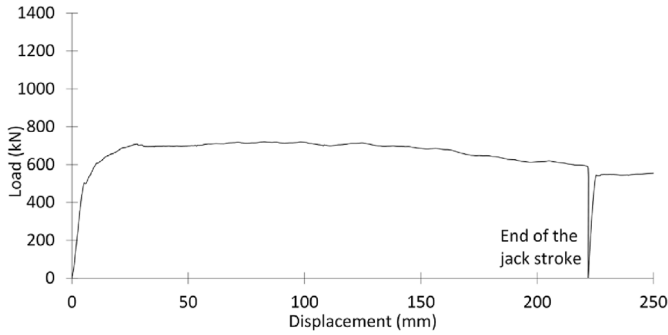
**Fig. 21.** Pullout load vs. displacement plot for anchor 4B: bond length 435 mm with debonding sleeve and $W/C = 0.55$. The load drop at around 220 mm marks the end of the stroke of the jack. Ultimate pullout load $P_{\text{ult}} = 720$ kN.
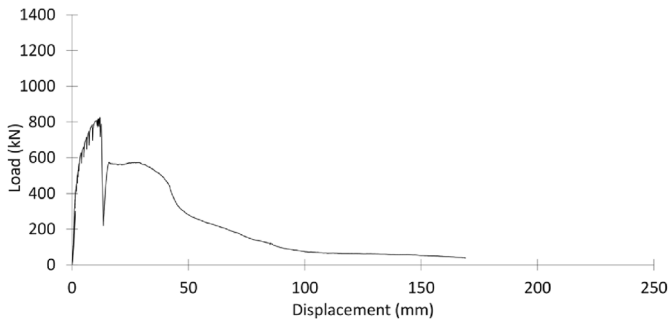


**Fig. 22.** Pullout load vs. displacement plot for anchor 1C: bond length 280 mm without debonding sleeve and $W/C = 0.42$. Ultimate pullout load $P_{\text{ult}} = 826$ kN.

the grout column moved up to 59 mm, implying that the grout column slipped significantly along the borehole wall, and the grout-rock interface must have been substantially damaged. The load along the entire anchor thread was constant and approximately 880 kN. The load transferred from the thread was $995 - 880 = 115$ kN.

The load distribution along the bond length of anchor 3C is shown in Fig. 24b for the four applied load levels. The load in the anchor was maximised at the top of the grout column and attenuated gradually to the endplate position. A small load, around 10% of the applied load, was transferred to the endplate until the applied load was approximately 90% (1238 kN) of the ultimate load. At the ultimate applied load (1376 kN), more than 90% of the applied load was transferred to the endplate. The evolution of the load distribution along anchor 3C was similar to that in anchor 2C, but the former carried a higher percentage of the applied load than the latter during the pre-peak stage. This is probably because of the long bond length (840 mm) of anchor 3C compared to that of anchor 2C (625 mm).

Based on the load distribution curves in Fig. 23b and 24b, the anchor thread carried the entire applied load during the linear load−displacement behaviour in the pre-peak stage. The endplate started to carry the load when the load−displacement curve began to yield. At the peak load, a large portion, >80%, of the applied load was transferred to the endplate. During the yielding stage, when the grout column slipped, the anchor thread still carried a small portion, about 10%, of the applied load.

## 4. Further discussions

### 4.1. Load models at the anchor-grout and grout-rock interfaces

The relationship between the axial stress $\sigma(x)$ in the anchor and the shear stress $\tau(x)$ on the anchor-grout interface can be derived by

considering the equilibrium of a small anchor element, as illustrated in Fig. 25 (Li, 2017). It is expressed as

$$\tau(x) = -\frac{A}{\pi d_{\text{b}}}\frac{\mathrm{d}\sigma(x)}{\mathrm{d}x} \tag{1}$$

where $\mathrm{d}\sigma(x)$ is the normal stress increment, $\mathrm{d}x$ is the element length, $d_{\text{b}}$ is the anchor diameter, and $A$ is the area of the cross-section of the anchor. The relationship between the axial normal stress in the grout column and the shear stress on the grout-rock interface is similar to the expression above, but the borehole diameter replaces the anchor diameter.

The shear stresses on both the anchor-grout and grout-rock interfaces can be obtained from the axial load measurements presented in the previous section according to Eq. (1). However, the shear stress obtained by this method fluctuates because of the discontinuities in the measured axial load data caused by the oversensitivity of the FBG sensors (the issue will be discussed in Section 4.5). Therefore, models for the distributions of the axial load along the anchor bond length and the shear stress along the interfaces are developed below with reference to the relationship expressed in Eq. (1).

#### 4.1.1. Load models along the anchor-grout interface for A-anchors

As shown in Fig. 10b, 11b and 13b and 15b, the axial pull load in the A-anchors was the largest at the top of the bonded length and attenuates abruptly to zero after a short distance downward in the grout when the applied load was low, such as less than 25% of the ultimate pullout load $P_{\text{ult}}$ (see Fig. 13b). The entire bond length was mobilised to carry load and the axial load in the anchor became approximately linearly decreasing toward the distal end of the anchor when the applied load was increased to approximately 50% of $P_{\text{ult}}$. After that, the distribution of the axial load in the anchor remained linear until the ultimate pullout load $P_{\text{ult}}$ is reached. This variation of the axial pull load in the A-anchors with increasing of the applied pull load is schematically sketched in Fig. 26a. In accordance with the relationship between the shear stress and the axial load described by Eq. (1), the shear stress on the cylindrical surface of the anchor is sketched in Fig. 26b. The shear stress exponentially decreases downward along the bond length at low levels of the applied load. It becomes linearly distributed along the bond length at approximately 50% of $P_{\text{ult}}$ with the zero shear stress at the distal end. After that, the shear stress on the portion of the bond length increases with an increase in the applied load. The shear stress becomes constant when the ultimate load $P_{\text{ult}}$ is reached and the bond length starts to slip.

The measurement data from the tests in this study agree in principle with the models for the shear stress distributions in Stage 1 and 3 in Fig. 1, but not in Stage 2. A short section of the bond length at the top might be debonded at a certain load level, but it was not observed that the debonding section extended toward the distal end with increasing of the applied load in the tests.

#### 4.1.2. Load models along the grout-rock interface for the debonded B-anchors

Strains in the grout column were measured for the debonded B-anchors 2B and 3B. The negative strains presented in Figs. 19b and 20b meant that the grout columns were subjected to compression. The axial compressive stress in the grout could be estimated from the measured strains according to the Hooke's law. It is seen in Fig. 20b that the curves of the strain are zigzag along the grout column possibly because of the sensitivity of the optical fibres which will be discussed in Section 4.5. In general, the compressive strain in the grout was the largest in a location slightly above the endplate. It then trended to attenuate toward the top of the grout
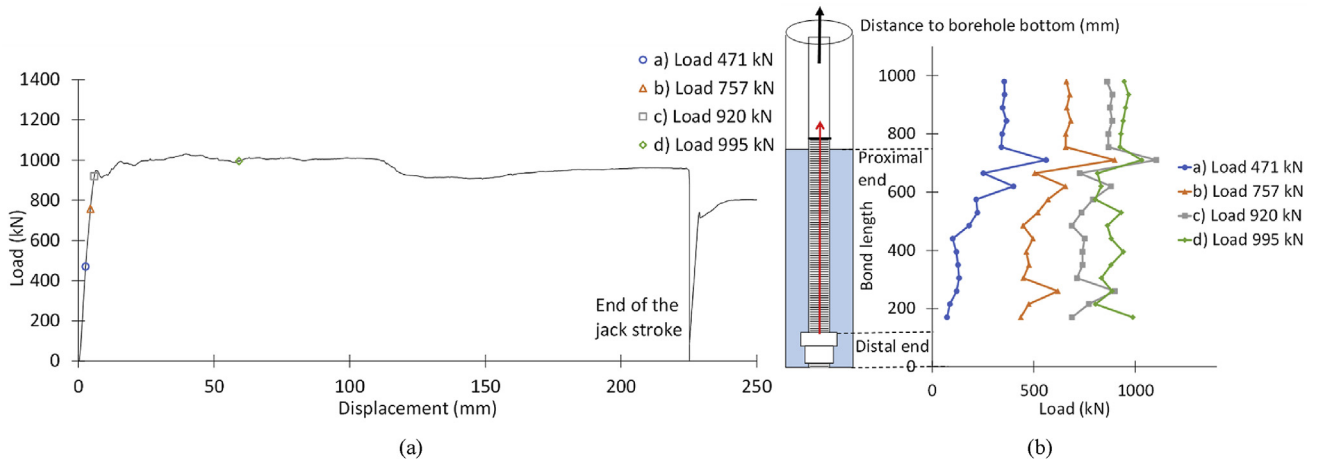
**Fig. 23.** Pullout test results for anchor 2C: bond length 625 mm without debonding sleeve and $W/C = 0.42$: (a) Load vs. displacement plot, and (b) Load distribution along the anchor. The load drop at around 220 mm marks the end of the stroke of the jack. Ultimate pullout load $P_{ult} = 1031$ kN.
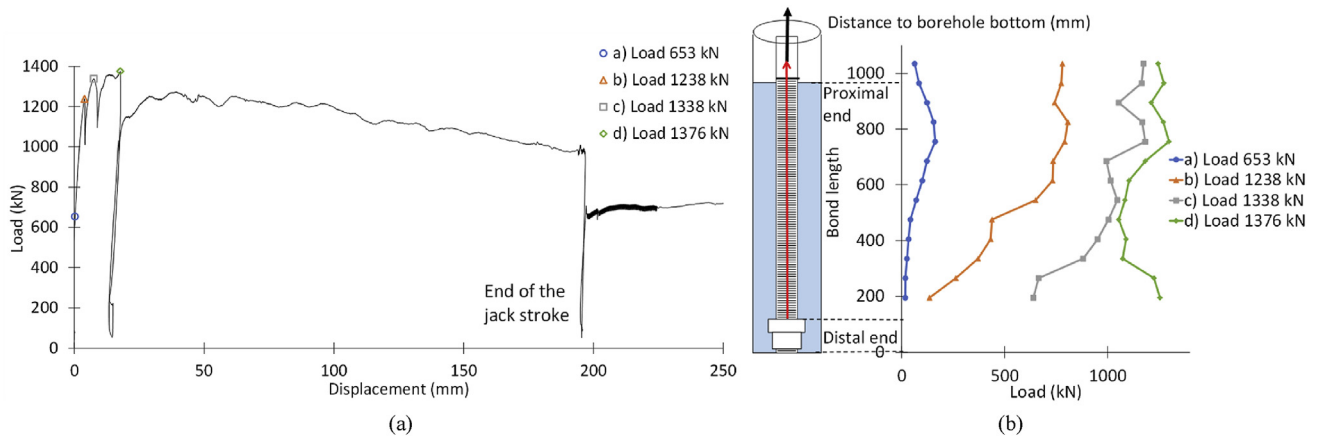


**Fig. 24.** Pullout test results for anchor 3C: bond length 840 mm without debonding sleeve and $W/C = 0.42$: (a) Load vs. displacement plot, and (b) Load distribution along the anchor. The load drop at around 200 mm marks the end of the stroke of the jack. Ultimate pullout load $P_{ult} = 1376$ kN.
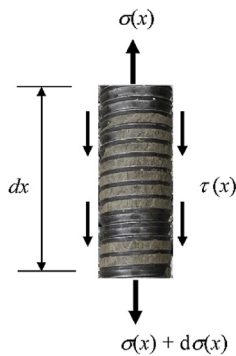


**Fig. 25.** Stress components on a small bolt element.
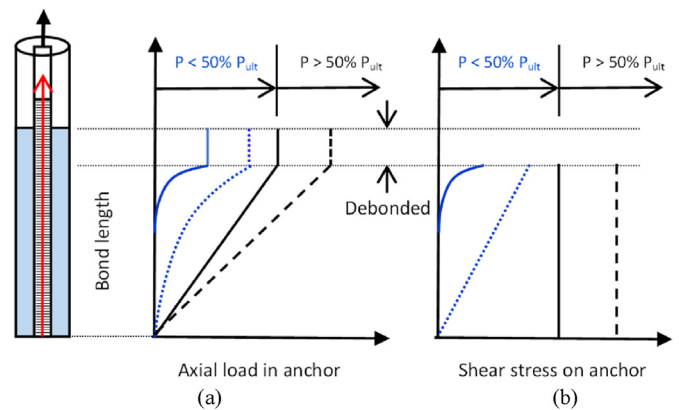


**Fig. 26.** Models for the axial load in the anchor (a) and for the shear stress on the anchor surface (b) (i.e. the anchor-grout interface) for A-anchors.

column. An exception was that the strain was approximately constant in the upper portion of the grout column at the load level of 637 kN for anchor 2B. That could be possible only when the top of the grout column was blocked to move, but such a blockage did not exist. The authors could not explain the exceptional phenomenon at this moment. All data presented in the two diagrams were measured in load levels between the yield load and the ultimate pull out load. Based on the known knowledge of the stress

distribution pattern along a rock anchor, one can infer that the strain in the grout should attenuate upward in a limited portion of the bond length at the elastic deformation stage. With this inference in mind and referring to the measurement data in Fig. 19b and 20b, the axial compressive stress in the grout column and the shear
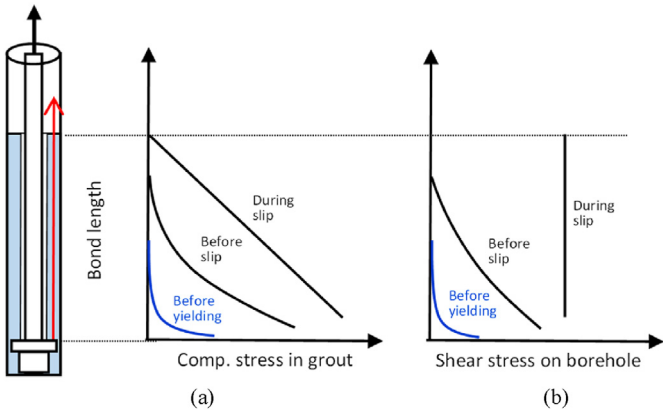
**Fig. 27.** Models for the compressive stress in the grout (a) and for the shear stress on the borehole wall (b) (i.e. the grout-rock interface) for the B-anchors.
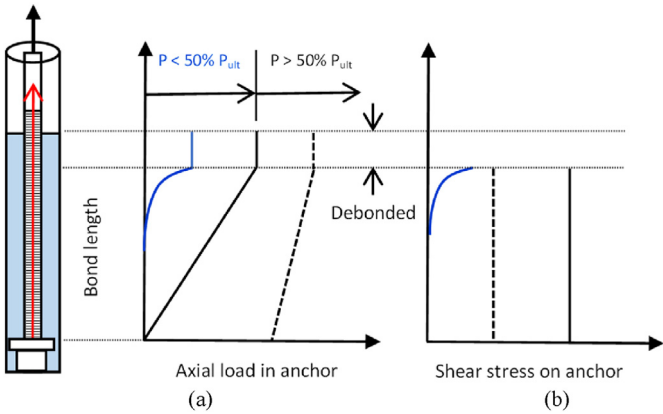


**Fig. 28.** Models for the axial load in the anchor (a) and the shear stress on the anchor surface (b) (i.e. the anchor-grout interface) for the non-debonded C-anchors.

stress on the borehole wall are schematically sketched in Fig. 27. The axial stress is the largest close to the endplate and decreases toward the top of the grout column. The variation of the compressive stress is nonlinear at the elastic deformation stage, but it becomes linear when the column start to slip along the borehole wall (Fig. 27a). The shear stress on the borehole wall, or on the grout-rock interface, is then constant during slippage (Fig. 27b). The absolute value of the constant shear stress during slippage

decreases during slippage with increasing of the damage on the borehole surface.

### 4.1.3. Load models along the anchor-grout interface for the non-debonded C-anchors

The variations of the axial pull load in the C-anchors 2C and 3C are presented in Figs. 23b and 24b, respectively. The entire bond length of the anchors was mobilised to carry load when the applied pull load was approximately 50% of $P_{ult}$, and the load decreases approximately toward the endplate, such as shown in Fig. 23b. The slope of the load distribution line was decreasing with increasing of the applied load. Based on these measurement results, the variations of the axial pull load in the C-anchor and the shear stress on borehole wall are schematically sketched in Fig. 28. The axial load in the anchor is the largest at the top of the bond length and attenuates toward the distal end of the anchor before slippage begins along the borehole wall (Fig. 28a). The load distribution becomes linear at approximately 50% of the $P_{ult}$. Afterward, the load at the endplate increases with increasing of the applied load, but the distribution remains linearly until the ultimate load is reached when the grout column starts to slip along the borehole wall. The distribution of the shear stress becomes approximately constant when the applied load reach 50% of $P_{ult}$ (Fig. 28b). After that, the constant value of the shear stress decreases with increasing of the applied load.

### 4.2. Load-transfer models

Ultimately, the anchor load transferred to the rock mass. The load-transfer patterns of the two types of anchors are illustrated in this section based on the test results from this study. Fig. 29 shows the models for the load transfer in the A-anchors in three loading stages. The load transferred to the rock mass at the grout-rock interface was the largest at the top of the bond length and attenuated approximately exponentially toward the distal end of the anchor when the applied load was very low, as shown in Fig. 29a. The entire bond length was mobilised to carry the load, and the load distribution decreased linearly when the applied load was approximately 50% of the ultimate load. The load distribution became uniform along the grout-rock interface when the grout column started to slip along the borehole wall (Fig. 29c). Under the axial pull load of the anchor, the stress state on the borehole wall is dominated by shear stress because the grout dilation is little and the dilation-induced normal stress is very low. With such a stress state, the major principal stress $\sigma_1$ transferred to the rock mass orients in an upward direction of approximately 45° to the borehole axis.
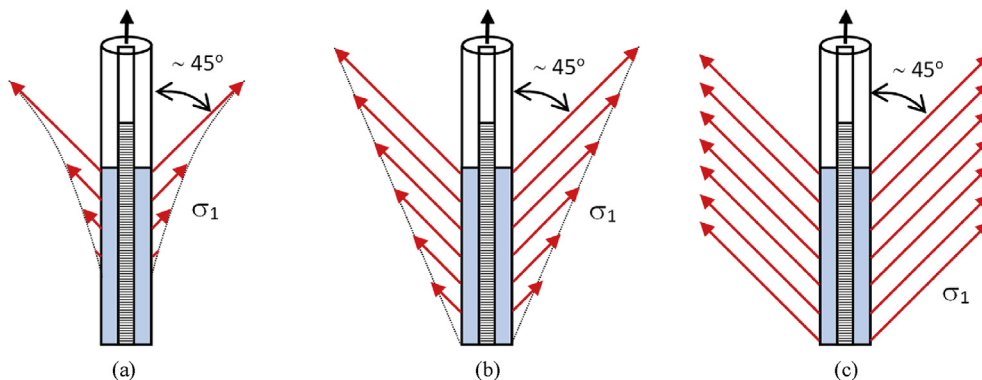


**Fig. 29.** Load-transfer patterns when the applied load is (a) $P << 50\% \ P_{ult}$, (b) $P \approx 50\% \ P_{ult}$, and (c) $P = P_{ult}$ and at the post-peak stage for A-anchors.
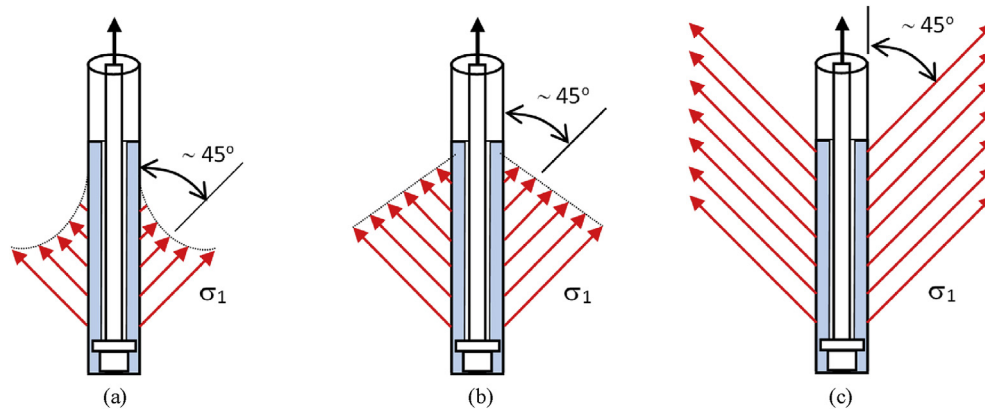
**Fig. 30.** Load-transfer patterns when the applied load is (a) $P << 50\% P_{ult}$, (b) $P \approx 50\% P_{ult}$, and (c) $P = P_{ult}$ and during slippage of the grout column for B- and C-anchors.



**Fig. 31.** Crushed grout in the borehole of anchor 3C after the endplate slid approximately 580 mm.

Fig. 30 shows the models for the load transfer of the B- and C-anchors in three loading stages. With these types of anchors, the load transferred to the rock mass was the largest slightly above the endplate and attenuated approximately exponentially upward when the applied load was very low (Fig. 30a). The entire bond length was mobilised to carry the load, and the load distribution increased linearly when the applied load was approximately 50% of the ultimate load. The load distribution became uniform along the grout-rock interface when the applied load equalled the ultimate load, as shown in Fig. 30c.

The bond length of the A-anchor is often much longer than the critical bond length in engineering practices. Thus, the loading pattern in Fig. 29a is valid for the engineering anchors. The main difference between the types of rock anchors is that the A-anchor transferred loads in the upper portion of the bond length, and the B- and C-anchors did so in the lower portion. The load-transfer patterns of the three types of anchors were identical when they started to slip along either the anchor-rock interface for the A-anchor or the grout-rock interface for the B- and C-anchors.

### 4.3. Failure of grout

Fig. 17 shows a hardened grout fragment after anchor 7A was pulled out of the borehole. The anchor thread was entirely cast in the mortar, as shown in Fig. 17a, indicating that the anchor-grout interface did not experience shear failure until the end of the test. Fig. 17b shows slick friction traces on the outer cylindrical surface of

the grout, implying that the grout column slid along the borehole wall. Therefore, the shear failure was on the grout-rock interface. It is inferred that the shear failure was mainly in the grout because the slick powder was dominated by grout cement, although limestone particles were also present. Hence, the shear strength of the grout-rock interface was decided by the strength of the grout.

Several parallel tiny fractures are visible on the rupture surface of the grout, as shown in Fig. 17a. The fractures started at the bottom of the anchor thread and propagated upward in the grout at an angle of around 35° to the anchor axis.

Fig. 31 shows the crushed grout in the borehole of anchor 3C after the endplate anchor was displaced upward by 580 mm. The grout was heavily fragmented, but the anchor was still carrying around 400 kN in this damaged state, which must be attributed to the normal stress on the borehole wall, which was induced by the dilation of the grout.

A grout cone is formed naturally above the endplate of the B- and C-anchors when the anchors slip along the borehole, as shown in Fig. 32 (see Fig. 8 for the initial shape of the endplate). The cone produces a lateral pressure on the borehole wall, increasing the friction resistance at the grout-rock interface. The grout cone is favourable, but the lateral pressure induced by it is unreliable because the cone could break, and the wedging effect would cease.

### 4.4. Estimation of bond shear strength

As presented in Section 3, the bond strength on the anchor-grout interface is around 20% of the UCS of the grout for the A-anchors. This bond strength may depend not only on the UCS of the grout but also on the configuration of the anchor thread. For individual rock anchors, obtaining the anchor-grout bond strength by pullout tests is preferable. The bond lengths used to obtain reliable test results for the three A-anchors were in the range of 485–730 mm (see Table 4), corresponding to 7.5–11.4 times the anchor thread diameter (64 mm). A scale effect is present, in that a shorter bond length leads to a larger strength, as shown by the blue dashed line in Fig. 33. Based on these results, it is recommended that the bond length should be at least 10–12 times the anchor thread diameter when the bond strength on the anchor-grout interface is tested in the field, corresponding to 640–768 mm for the 64-mm anchor.

Among the anchors installed using the grout with $W/C = 0.42$, three A-anchors, two B-anchors, and two C-anchors failed along the grout-rock interface (Tables 4–6). The failure appeared mostly in the grout. The average bond shear strength of the grout-rock interface was 5.34% of the UCS of the grout for the three A-
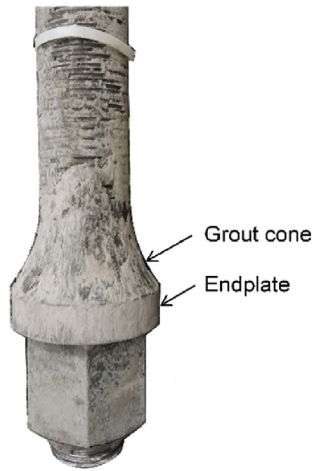
**Fig. 32.** The grout cone formed above the endplate of a C-anchor after pullout of the anchor.

anchors and 6.56% for the four B- and C-anchors. The bond strengths obtained for the B- and C-anchors were slightly larger than those for the A-anchors (Fig. 33), possibly because of the greater dilation normal pressure induced by the grout cone in the B- and C-anchor tests. The bond shear strength on the grout-rock interface was also scale-dependent, but the scale effect was very weak, as shown by the black dashed line in Fig. 33. The current rock anchor design uses 10% of the UCS of the rock for the bond strength of the grout-rock interface (Littlejohn, 1992). The failure in this study was not necessarily in the rock but could have occurred in the grout, as appeared in the tests of our study. It is not always appropriate to estimate the bond strength from the UCS of the rock, as suggested by Littlejohn (1992). Based on the test results in our study, a reasonable bond shear strength is approximately 5% of the UCS of the grout or rock, whichever is weaker.

### 4.5. Fibre measurements

Fibre optic cables were used to monitor the strains along some of the anchors. The fibres had 20 FBG sensors distributed evenly along the bond length of the anchors. These fibre optic cables were very brittle and required careful handling. The two first anchors with fibre optic cables broke before the tests started. In the remaining tests, the fibres showed mostly good performance at the

elastic stage of the anchor test with some measurement uncertainty. At the plastic stage, the measurements started to vary more (see green curves in Figs. 10b and 11b), and after bond failure and crushing of the grout, the measurements had large fluctuations and were unreliable. Some of the fibres failed during the tests. These large variations in the measurements could be associated with dilation in the grout as the anchor was pulled out. In the soil anchor tests by Smet et al. (2019) and Fabris et al. (2021), likely, the grout was not crushed, and the fibres were therefore not exposed to dilation, which may be the reason why fibre optic cables work well in soil applications.

## 5. Conclusions

Pullout tests of three types of rock anchors were conducted in a limestone quarry to investigate the bond strengths of the anchor-grout and grout-rock interfaces and the shear failure process along these interfaces.

For the A-anchor, which is anchored in the grout by threads, the shear stress on the anchor-grout interface is the largest at the top of the grout column and attenuates toward the distal end of the anchor as loading begins. The shear stress becomes uniformly distributed over the entire bond length when the applied load is approximately 50% of the ultimate pullout load.

For B- and C-anchors, which has an endplate in the distal end of the anchor, the shear stress on the grout-rock interface is the largest at the endplate and attenuates upward toward the top of the grout column before slip starts along the interface. The shear stress becomes approximately constant when the ultimate pullout load is reached, and the grout column starts to slip along the interface.

The bond shear strength on the anchor-grout interface was approximately 20% of the UCS of the grout in the tests. The bond strength is also associated with the configuration of the anchoring thread. Pullout tests should be carried out for a specific type of anchor. The recommended bond length for the pullout test is 10−12 times the anchor diameter.

The bond shear strength on the grout-rock interface was between 5.34% and 6.56% of the UCS of the grout in the tests. The grout-rock bond strength is possibly determined by the strength of the grout or rock, whichever is weaker. A reasonable estimation of the bond shear strength on the grout-rock interface may be 5% of the UCS of the grout or the rock, whichever is weaker.

These tests show that optical measurements are too sensitive for pullout tests of rock anchors, likely due to the lateral pressure from dilation in the crushed grout. The authors, therefore, recommend
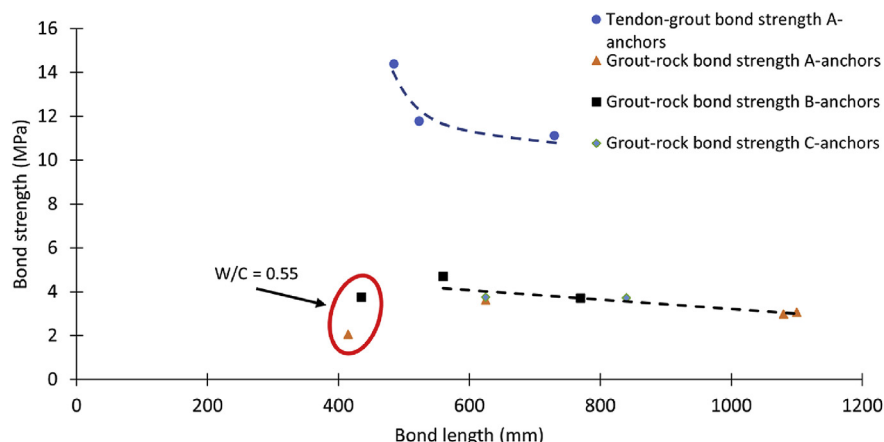


**Fig. 33.** Bond strength plotted against bond length for the valid tests.

using well-tested technologies, such as strain gauges, for similar tests to obtain reliable results.

## Data availability

The datasets generated during the current study are available from the corresponding author on reasonable request.

## Declaration of competing interest

The authors declare that they have no known competing financial interests or personal relationships that could have appeared to influence the work reported in this paper.

## Acknowledgments

## References

Benmokrane, B., Ballivy, G., 1991. Five-year monitoring of load losses on prestressed cement-grouted rock anchors. Can. Geotech. J. 28, 668–677.

Benmokrane, B., Chekired, M., Xu, H., 1995. Monitoring behavior of grouted anchors using vibrating-wire gauges. J. Geotech. Eng. 121, 466–475.

Briaud, J.L., Powers, W.F., Weatherby, D.E., 1998. Should grouted anchors have short tendon bond length? J. Geotech. Geoenviron. Eng. 124, 110–119.

Brown, E.T., 2015. Rock engineering design of post-tensioned anchors for dams - a review. J. Rock Mech. Geotech. Eng. 7, 1–13.

Bruce, D.A., 1976. The Design and Performance of Prestressed Rock Anchors with Particular Reference to Load Transfer Mechanisms (As Reproduced by ProQuest LLC 2014 (UMI U433767)). PhD Thesis. University of Aberdeen, Aberdeen, Scotland.

Bruce, D.A., 1997. The stabilization of concrete dams by post-tensioned rock anchors: the state of American practice. In: Ground Anchorages and Anchored Structures: Proceedings of the International Conference. Thomas Telford Publishing, London, England, pp. 508–521.

Bryson, L.S., Giraldo, J.R., 2019. Analysis of case study presenting ground anchor load-transfer response in shale stratum. Can. Geotech. J. 57, 85–99.

Dados, A.T., 1984. Design of anchors in horizontally jointed rocks. J. Geotech. Eng. 110, 1637–1647.

Fabris, C., Schweiger, H.F., Pulko, B., Woschitz, H., Račanský, V., 2021. Numerical simulation of a ground anchor pullout test monitored with fiber optic sensors. J. Geotech. Geoenviron. Eng. 147, 147.

Farmer, I.W., 1975. Stress distribution along a resin grouted rock anchor. Int. J. Rock Mech. Min. Sci. Geomech. Abstr. 12, 347–351.

Haberfield, C.M., Baycan, S., 1997. Field performance of the grout/rock interface in anchors. In: Ground Anchorages and Anchored Structures: Proceedings of the International Conference. Thomas Telford Publishing, London, England, pp. 45–54.

Hanna, T.H., 1982. Foundations in Tension: Ground Anchors. Trans Tech Publications and McGraw-Hill Book Company, Clausthal, Germany.

Hobst, L., Zajíc, J., 1983. Anchoring in Rock and Soil. Elsevier Scientific Publishing Company, New York, USA.

Hollingshead, G.W., 1971. Stress distribution in rock anchors. Can. Geotech. J. 8, 588–592.

Ismael, N.F., 1982. Design of shallow rock-anchored foundations. Can. Geotech. J. 19, 46–3471.

Ismael, N.F., Radhakrishna, H.S., Klym, T.W., 1979. Uplift capacity of rock anchor groups. IEEE Trans. Power Apparatus Syst. 98, 1653–1658.

Kim, D.H., Lee, S.R., 2005. Uplift capacity of fixed shallow anchors subjected to vertical loading in rock. Int. J. Offshore Polar Eng. 15, 312–320.

Kim, H.K., Cho, N.J., 2012. A design method to incur ductile failure of rock anchors subjected to tensile loads. Electron. J. Geotech. Eng. 17, 2737–2746.

Li, C., Stillborg, B., 1999. Analytical models for rock bolts. Int. J. Rock Mech. Min. Sci. 36, 1013–1029.

Li, C.C., 2017. Rockbolting: Principles and Applications. Butterworth-Heinemann, Elsevier.

Littlejohn, G.S., 1992. Rock anchorage practice in civil engineering. In: Balkema, A.A. (Ed.), Rock Support in Mining and Underground Construction: Proceedings of the International Symposium on Rock Support, pp. 257–268. Sudbury, Ontario, Canada.

Littlejohn, G.S., Bruce, D.A., 1977. Rock Anchors - State of the Art. Foundation publications Ltd., Brentwood, Essex, England.

Littlejohn, G.S., Bruce, D.A., Deppner, W., 1978. Anchor field tests in carboniferous strata. Rev. Fr. Geotech. 3, 82–86.

Liu, X., Wang, J., Huang, J., Jiang, H., 2017. Full-scale pullout tests and analyses of ground anchors in rock under ultimate load conditions. Eng. Geol. 228, 1–10.

Liu, X., Zhou, Y., Chen, C., Zhen, Y., Xia, K., 2013. Anchoring characteristic of tension-type anchor cable and grout length design. In: Rock Characterisation, Modelling and Engineering Design Methods. CRC Press, Shanghai, China, pp. 697–702.

Panton, B., Elmo, D., Carvalho, J., Brown, E.T., 2015. Numerical simulation of rock cone pullout and the influence of discrete fracture network statistics on foundation anchor capacity. In: 13th International Congress of Rock Mechanics. International Society for Rock Mechanics, Montreal, Canada, p. 11.

Park, J., Qiu, T., Kim, Y., 2013. Field and laboratory investigation of pullout resistance of steel anchors in rock. J. Geotech. Geoenviron. Eng. 139, 2219–2224.

Pease, K.A., Kulhawy, F.H., 1984. Load Transfer Mechanisms in Rock Sockets and Anchors. Project 1493-1 EPRI EL-3777. Electric Power Research Institute, Ithaca, New York, USA.

Pedersen, A.H., 2014. Large-Scale Underground Mining in Tromsdalen. MSc Thesis. Norwegian University of Science and Technology (NTNU), Trondheim, Norway.

Scott, G.A., Bruce, D.A., 1992. Full scale field tests of high capacity rock anchors. In: The 33rd U.S. Symposium on Rock Mechanics. A.A. Balkema, Santa Fe, New Mexico, USA, pp. 471–480.

Smet, J., Huybrechts, N., Lysebetten, G.V., Verstraelen, J., François, S., 2019. Optical fiber strain measurements and numerical modeling of load tests on grouted anchors. J. Geotech. Geoenviron. Eng. 145, 19.

Storli, A.M., 2021. Tromsdalen. Franzefoss Minerals. https://kalk.no/selskap-og-anlegg/verdalskalk/tromsdalen/. (Accessed 12 October 2021).

Tayeh, B.A., El dada, Z.M., Shihada, S., Yusuf, M.O., 2019. Pull-out behavior of post installed rebar connections using chemical adhesives and cement based binders. J. King Saud Univ. Eng. Sci. 31, 332–339.

Thomas-Lepine, C., 2012. Rock Bolts - Improved Design and Possibilities. MSc Thesis. Norwegian University of Science and Technology (NTNU), Trondheim, Norway.

Vukotic, G., Galindo, J.G., Soriano, A., 2013. The influence of bond stress distribution on ground anchor fixed length design. Field trial results and proposal for design methodology. In: Proceedings of the 18th International Conference on Soil Mechanics and Geotechnical Engineering: Challenges and Innovations in Geotechnics. Presses des Ponts, Paris, France, pp. 2119–2122.

Weerasinghe, R.B., Littlejohn, G.S., 1997. Uplift capacity of shallow anchorages in weak mudstone. In: Ground Anchorages and Anchored Structures: Proceedings of the International Conference. Thomas Telford Publishing, London, England, pp. 23–33.

Xanthakos, P.P., 1991. Ground Anchors and Anchored Structures. Wiley Interscience, John Wiley & Sons, Inc., New York, USA.

Xiao, T., He, Y., 2018. Experimental study of an inflatable recyclable anchor. Adv. Mater. Sci. Eng. 10, 2018.

Zhu, H.H., Shi, B., Zhang, C.C., 2017. FBG-based monitoring of geohazards: current status and trends. Sensors 17, 452–474.

**Bjarte Grindheim** obtained his MSc degree in Rock Mechanics and Rock Engineering from Norwegian University of Science and Technology (NTNU), Norway, in 2020, and started his PhD in Rock Mechanics and Rock Engineering at NTNU in 2020. He was awarded Vår Energi's scholarship for highest grade average in his year of the Masters in Geotechnology. He is a member of the International Society for Rock Mechanics and Rock Engineering (ISRM). His research interests are within rock anchoring.